

Unveiling temperature dependence mechanisms of perpendicular magnetic anisotropy at Fe/MgO interfaces

Fatima Ibrahim,^{1,*} Ali Hallal,¹ Alan Kalitsov,² Bernard Dieny,¹ and Mairbek Chshiev^{1,3,†}

¹*Univ. Grenoble Alpes, CEA, CNRS, SPINTEC, 38000 Grenoble, France*

²*Western Digital Technologies, Inc., 5601 Great Oaks Parkway, San Jose, CA 95119, USA*

³*Institut Universitaire de France*

The perpendicular magnetic anisotropy at magnetic transition metal/oxide interfaces is a key element in building out-of-plane magnetized magnetic tunnel junctions for spin-transfer-torque magnetic random access memory (STT-MRAM). Size downscaling renders magnetic properties more sensitive to thermal effects. Thus, understanding the temperature dependence of the magnetic anisotropy becomes crucial. In this work, we theoretically address the correlation between temperature dependence of magnetic anisotropy and magnetization in typical Fe/MgO-based structures. In particular, the possible mechanisms behind the experimentally-reported deviations from the Callen and Callen scaling power law are analyzed. First-principles calculations reveal small high-order anisotropy constants compared to first order, thus ruling out an intrinsic microscopic mechanism underlying those deviations. Neglecting higher-order anisotropy terms in the atomistic spin Hamiltonian, two possible extrinsic macroscopic mechanisms are unveiled namely the influence of the dead layer, always present in the storage layer of STT-MRAM cells, and the spatial inhomogeneities of the interfacial magnetic anisotropy. About the first mechanism, we show that the presence of a dead layer simultaneously with scaling the anisotropy constant, which is interfacial, by the total magnetization of the sample rather than that of the interface itself lead to low scaling powers. In the second mechanism, increasing the percentage of inhomogeneity in the interfacial perpendicular magnetic anisotropy is revealed to decrease the scaling power. Apart from those different mechanisms, the layer-resolved temperature-dependence of anisotropy is shown to ideally follow the Callen and Callen scaling power law for each individual Fe layer. These results allow to coherently explain the difference in scaling powers relating anisotropy and magnetization thermal variations reported in earlier experiments. This is crucial for the understanding of the thermal stability of the storage layer magnetization in STT-MRAM applications.

I. INTRODUCTION

The evolution in the magnetic random access memories (MRAM) technologies was made possible thanks to the fundamental research breakthroughs in spintronic phenomena and materials development. Intensive efforts focus on spin transfer torque (STT) [[1, 2]] that enables current-induced switching and thus better downscalability compared to field-written MRAM [[3–6]]. More precisely, perpendicular STT-MRAMs where out-of-plane magnetized magnetic tunnel junctions serve as storage elements provide both low switching currents, owing to the relatively weak Gilbert damping, and high thermal stability thanks to their large perpendicular magnetic anisotropy (PMA) values [[7–9]]. PMA was observed to be common at magnetic metal/oxide interfaces with either amorphous or crystalline oxides [[10–12]] and was theoretically attributed to the electronic hybridization between the oxygen and magnetic transition metal orbitals across the interface [[13]].

The memory retention which is determined by the thermal stability of the storage layer magnetization is directly related to this layer's PMA. This is a key

parameter in STT-MRAM applications. The concept of thermally assisted STT-MRAM was also proposed to reduce the write current while maintaining a large thermal stability factor [[14]]. In regards to applications, the sensitivity of magnetic properties to temperature is a critical point especially for applications having to operate on a broad range of temperature such as the automotive ones. This emphasizes the need for a fundamental understanding of the PMA dependence on temperature. In this context, the correlation between temperature-dependent anisotropy constant K and magnetization M of ferromagnets, as described by Callen and Callen, follows a power scaling law: $\frac{K(T)}{K(0)} = \left[\frac{M(T)}{M(0)} \right]^n$ with $n = i(2i + 1)$ corresponding to the i th order anisotropy constant [[15, 16]]. It follows that for the first order anisotropy constant K_1 , a scaling power $n = 3$ is expected. However, deviations from this law with scaling powers $n < 3$ have been experimentally reported [[17–19]]. This was explained by the two-ion anisotropy model in L_{10} FePt alloys [[20, 21]] and more recently in CoFeB/MgO structures [[19]]. However, considering various mechanisms that are likely to occur in actual devices and their probable contribution to the temperature dependence of the magnetic properties, the analysis of the relationship between thermal variations of anisotropy and magnetization requires further clarification. For instance, the effect of magnetic dead layer, which often forms when using buffer or

* fatima.ali.ibrahim@hotmail.com

† mair.chshiev@cea.fr

capping layers for transition metal/oxide structures [[22]], has so far not addressed. Since the thickness of the dead layer is temperature dependent, considering its effect on the correlation between temperature dependences of K and M becomes essential. Another possible effect is the spatial thickness fluctuations at the interface [[23]] giving rise to a second-order anisotropy K_2 contribution manifested as a canted or easy cone magnetic states [[24]]. All this emphasizes the importance of clarifying the mechanisms contributing to the temperature dependence of magnetic anisotropy and whether they are micro- or macroscopic in nature. In particular, the mechanisms underlying deviations from the theoretical Callen-Callen power law require further investigation.

In this paper, we study theoretically the correlation between temperature dependences of magnetic anisotropy and magnetization in typical Fe/MgO-based structures addressing several fundamental and practical aspects. Our first-principles calculations carried out on ideal structure reveal that the second order magnetic anisotropy constant K_2 is one order of magnitude smaller than its first order one K_1 indicating that the presence of higher-order anisotropy terms is not intrinsic. Neglecting higher-order anisotropy contributions to the atomistic spin Hamiltonian, calculations were performed in order to unveil the macroscopic mechanisms of temperature dependence of magnetic anisotropy. First, we elucidate that its layer-resolved behavior does follow the Callen and Callen scaling power law with $n = 3$ provided that the interfacial anisotropy is scaled with the magnetization of the interfacial magnetic layer and not with that of the whole magnetic layer. Next, two mechanisms that are very likely to occur in magnetic metal/oxide structures are considered and their impact on the correlation between temperature dependences of K and M is explored. It is shown that the presence of a magnetic dead layer together with scaling the anisotropy constant by the total magnetization of the sample rather than the magnetization of the interface itself is shown to yield lower scaling powers deviating from the theoretical law. The second mechanism reveals that increasing the percentage of inhomogeneity in the interfacial PMA decreases the scaling power. The present results elucidate that the mechanisms behind the deviations from the theoretical Callen-Callen power law are extrinsic (presence of a dead layer and of interfacial roughness) rather than intrinsic. These results allow to coherently explain the difference in scaling powers relating anisotropy and magnetization thermal variations reported in earlier experiments.

II. K_1 AND K_2 EVALUATION FROM FIRST-PRINCIPLES

The interfacial magnetic anisotropy energy MAE is obtained from the dependence of the total energy E on the angle θ between the magnetization direction and the

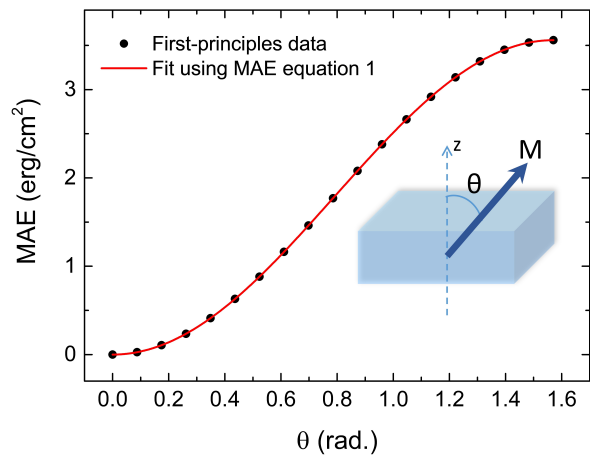


FIG. 1. (Color online) The magnetic anisotropy energy as a function of the angle θ between the magnetization direction and the normal to the interface calculated for Fe/MgO structure by first-principles (data points) is fitted to the MAE Eq. 1 (solid line).

normal to the interface expressed as:

$$MAE(\theta) = E(\theta) - E(0) = K_1 \sin^2 \theta + K_2 \sin^4 \theta + K_3 \sin^6 \theta + \dots = \sum K_i \sin^{2i} \theta. \quad (1)$$

Typically, the first order term K_1 dominates the higher order ones in structures with interfacial anisotropy. However, experiments have observed the influence of the second order K_2 , namely in the formation of an easy-cone state [[24, 25]]. The origin of significant K_2 values is attributed to spatial fluctuations of the film thickness [[23, 26]], strongly interface-concentrated PMA combined to a moderate exchange coupling of the interface moment to the rest of the film [[27]] or strong magnetic inhomogeneities [[28]]. Although aforementioned experiments were explained by such extrinsic mechanisms, it is necessary to elucidate whether the higher-order anisotropy terms may also be of intrinsic origin. For this, we performed systematic first-principles calculations to quantify the higher-order anisotropy terms in MgO-based interfaces including Fe/MgO and FeCo/MgO with either Co or FeCo termination.

	Fe/MgO	FeCo/MgO	FeCo/MgO
Termination	Fe	Co	FeCo
K_1 (erg/cm ²)	3.52	0.45	0.87
K_2 (erg/cm ²)	0.038	0.077	0

TABLE I. The first order K_1 and second order K_2 anisotropy obtained for Fe/MgO and FeCo/MgO with either Co- or FeCo-terminated structures by fitting the first-principles calculated MAE to Eq. (1).

The total energies from first-principles calculations were fitted with Eq. (2) up to the third order. As an

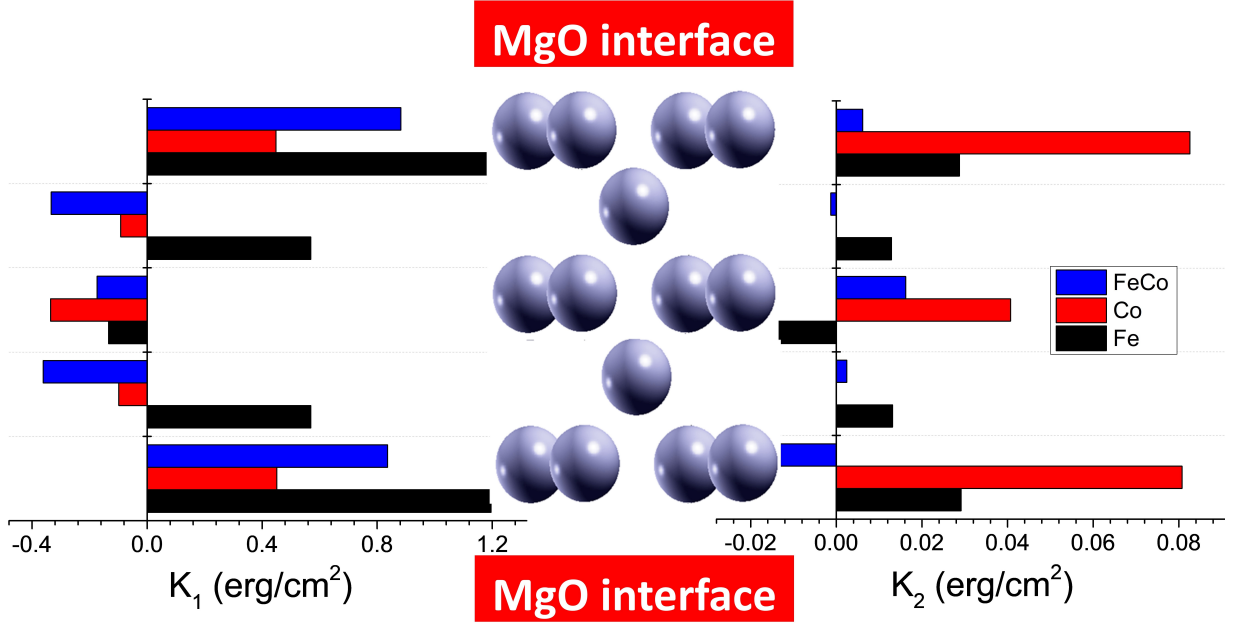


FIG. 2. (Color online) Layer-resolved values of K_1 and K_2 , obtained from first-principles calculations, are compared for Fe/MgO and FeCo/MgO with either Co- or FeCo-terminated interfaces.

example, in Fig. 1 we show for the case of Fe/MgO structure. The obtained K_1 and K_2 values for interfaces studied are summarized in Table II. One can observe that: (i) both K_1 and K_2 values are dependent on the interface termination while (ii) K_2 is found to be one order of magnitude smaller than K_1 and (iii) K_3 values are found to be negligible for all cases. Of note, similar K_2 to K_1 ratios were reported for FePt by first-principles calculations [[29]].

To get more insights, in Fig. 2 we present the layer-resolved K_1 and K_2 values for different interfaces studied. In case of Fe/MgO K_1 is not entirely localized at the interface but rather propagates into the bulk showing an attenuating oscillatory behavior [30]. The layer-resolved K_2 for this structure follows the K_1 in trend and sign. The situation is different in the case of FeCo/MgO interface showing that for all terminations K_1 is overall lower compared to that at Fe/MgO and PMA originates from the first layer. As for the K_2 , it is positive and one order of magnitude smaller than K_1 for Co-terminated interface, while it is negligible and depend strongly on the atomic distribution for FeCo-terminated interface.

Based on these findings, we conclude that significant K_2 are not of intrinsic origin in MgO-based interfaces and its emergence should be attributed to extrinsic mechanisms. In particular, fluctuations of interfacial PMA were pointed out by experiments [28] and modeled analytically [26] or by macrospin approximation [31] giving rise to significant K_2 values. Thus, in order to address the temperature dependence of magnetic anisotropy, we exclude K_2 from the atomistic spin

Hamiltonian. In the following we focus instead on exploring two extrinsic mechanisms that are commonly encountered in experiments, namely the presence of a magnetic dead layer and of spatial inhomogeneities in the interfacial PMA.

III. LAYER-RESOLVED TEMPERATURE DEPENDENCE OF MAGNETIC ANISOTROPY

Before investigating the mechanisms that contribute to the temperature dependence of magnetic anisotropy, let us first address the fundamental aspect of its layer-resolved behavior for Fe/MgO interface. We start with the simple model where the system comprises one Fe layer with interfacial magnetic anisotropy (Fe1) and the bulk region with negligible anisotropy of total thickness $t = 2$ nm [Fig. 3(a)]. The normalized saturation magnetization M_s of Fe1 decreases more rapidly with temperature compared to that of the bulk as shown in Fig. 3(b) due to the reduced atomic coordination at the interface. Next, we fit and compare the calculated anisotropy $K(T)$ to $M_s(T)$ in two cases. If the total saturation magnetization $M_{total}(T)$ is considered we obtain a scaling power $n = 4.9$ [Fig. 3(c)]. However, using the interface saturation magnetization $M_{Fe1}(T)$ yields $n = 3$, i.e. $\frac{K_{Fe1}(T)}{K_{Fe1}(10K)} = \left[\frac{M_{Fe1}(T)}{M_{Fe1}(10K)} \right]^3$ following exactly the Callen-Callen law [Fig. 3(d)]. The latter case is more justified since the anisotropy is of interfacial origin and more precisely contributed by Fe1 in this case.

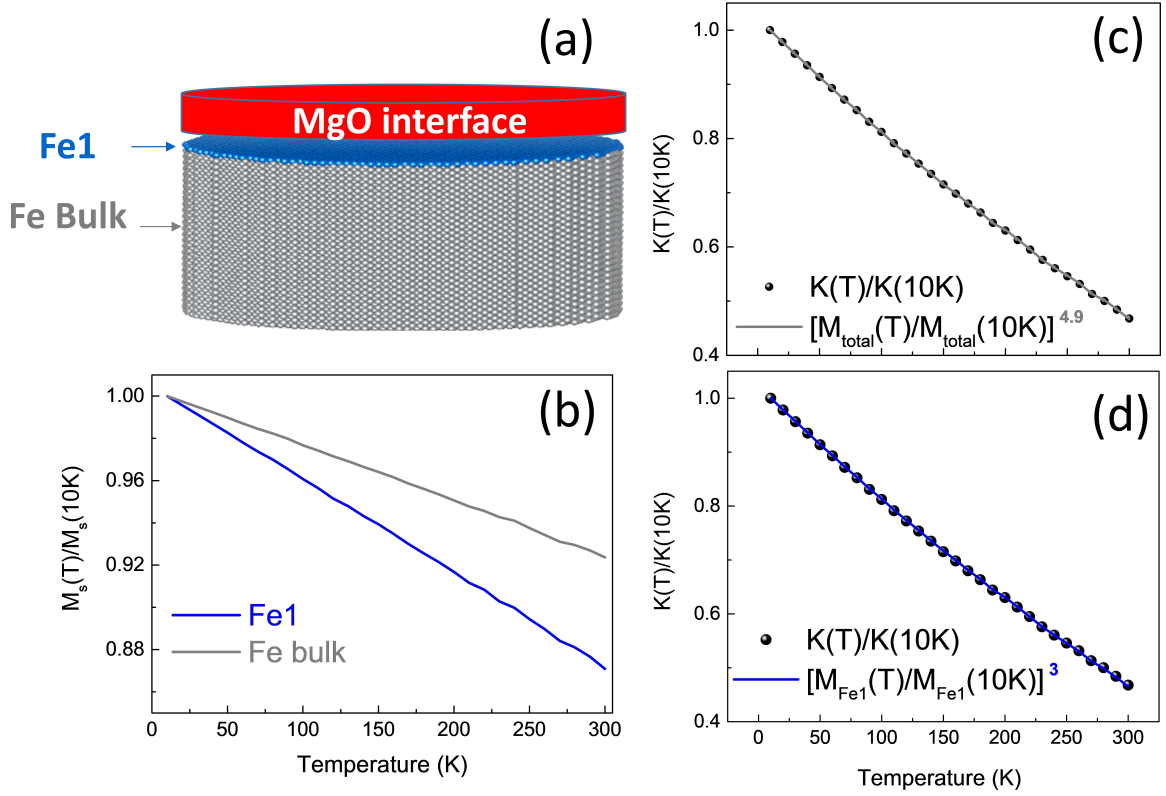


FIG. 3. (Color online) (a) The model Fe/MgO structure used to calculate the temperature-dependent magnetic properties comprising a bulk Fe region and one interfacial layer (Fe1). (b) The normalized saturation magnetization M_s per region is plotted as a function of temperature. The normalized magnetic anisotropy K as a function of temperature is shown with its fit to the normalized saturation magnetization of the whole structure M_{total} (normalized saturation magnetization of the interfacial Fe1 layer M_{Fe1}) yielding a scaling power $n = 4.9$ ($n = 3$) shown in c (d), respectively.

Next, we improve the model by including the interfacial anisotropy values for both the first Fe1 and second Fe2 monolayers obtained from the first-principles with a bulk region and total thickness of 2 nm. Fig. 4(a) compares the layer-resolved saturation magnetization for three different regions. While the decrease of the Fe1 magnetization as a function of temperature is steeper than that in the bulk, the Fe2 magnetization follows almost the same behavior as in the bulk. This is also explained by the reduced atomic coordination for Fe1

layer which is not the case for Fe2. Since both Fe1 and Fe2 contribute to the interfacial anisotropy, we then fit $K_{Fe1+Fe2}(T)$ to the average saturation magnetization of both layers $M_{Fe1+Fe2}(T)$. In this case, a scaling power $n = 3.3$ is obtained.

To extract per layer resolved correlation between $K(T)$ and $M_s(T)$, the results of previous two models are used. Considering two interfacial Fe monolayers, the expression of the temperature-dependent anisotropy can be expanded as:

$$\frac{K_{Fe1+Fe2}(T)}{K_{Fe1+Fe2}(10K)} = \frac{K_{Fe1}(T)}{K_{Fe1}(10K)} \left[\frac{K_{Fe1}(10K)}{K_{Fe1}(10K) + K_{Fe2}(10K)} \right] + \frac{K_{Fe2}(T)}{K_{Fe2}(10K)} \left[\frac{K_{Fe2}(10K)}{K_{Fe1}(10K) + K_{Fe2}(10K)} \right]. \quad (2)$$

Assuming that the magnetic anisotropy of every Fe layer i (K_{Fe_i}) scales as $n = 3$ with its saturation magnetization

M_{Fe_i} according to the Callen-Callen power law, Eq. (2) can be rewritten as

$$\frac{K_{Fe1+Fe2}(T)}{K_{Fe1+Fe2}(10K)} = \left[\frac{M_{Fe1}(T)}{M_{Fe1}(10K)} \right]^3 \left[\frac{K_{Fe1}(10K)}{K_{Fe1}(10K) + K_{Fe2}(10K)} \right] + \left[\frac{M_{Fe2}(T)}{M_{Fe2}(10K)} \right]^3 \left[\frac{K_{Fe2}(10K)}{K_{Fe1}(10K) + K_{Fe2}(10K)} \right]. \quad (3)$$

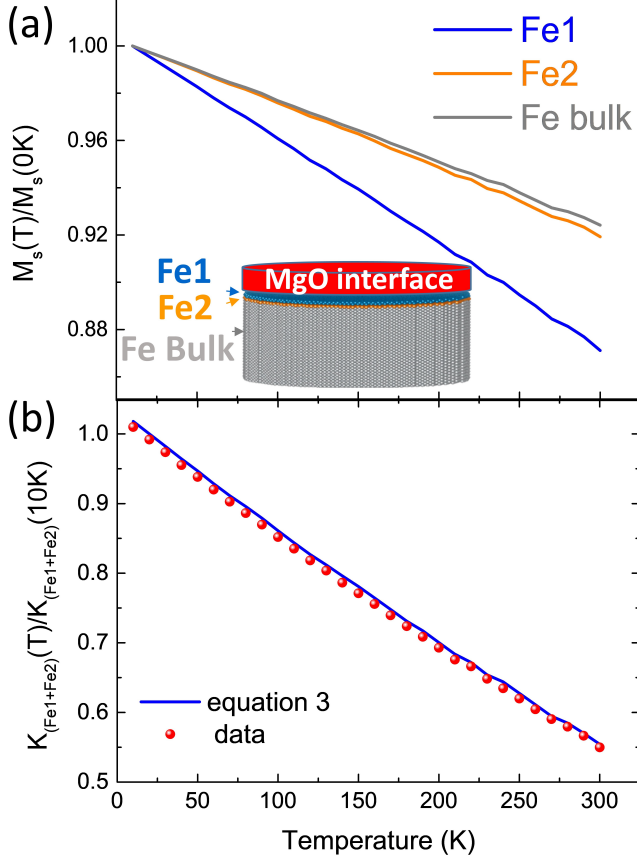


FIG. 4. (Color online) (a) The normalized saturation magnetization M_s per region as a function of the temperature for the model Fe/MgO structure used to calculate the temperature dependent magnetic properties comprising a bulk Fe region and two interfacial layers (Fe1 and Fe2). (b) The normalized magnetic anisotropy $K_{Fe1+Fe2}$ as a function of temperature considering the model in Fig 4 is shown by circle data points. The solid line corresponds to Eq. 3.

The calculated data accounting for the anisotropy of both Fe1 and Fe2 that yields $n = 3.3$ are then compared to those obtained using Eq. 3 [Fig. 4(b)]. The excellent agreement between two curves confirms the validity of our assumption that the layer-resolved behavior follows the Callen-Callen scaling power law for each individual Fe layer: $\frac{K_{Fe_i}(T)}{K_{Fe_i}(10K)} = \left[\frac{M_{Fe_i}(T)}{M_{Fe_i}(10K)} \right]^3$.

IV. EFFECT OF MAGNETIC DEAD LAYER

Magnetic dead layers form when the atoms of the capping or buffer layer diffuse into the magnetic region upon annealing resulting in a reduced coordination. We therefore chose to model the dead layer by introducing a gradient of the exchange interaction (or stiffness) constant in the outermost four Fe layers opposite to the Fe/MgO interface [see the inset of Fig. 5]. We find that the estimated dead layer thickness t_{dead} is negligible

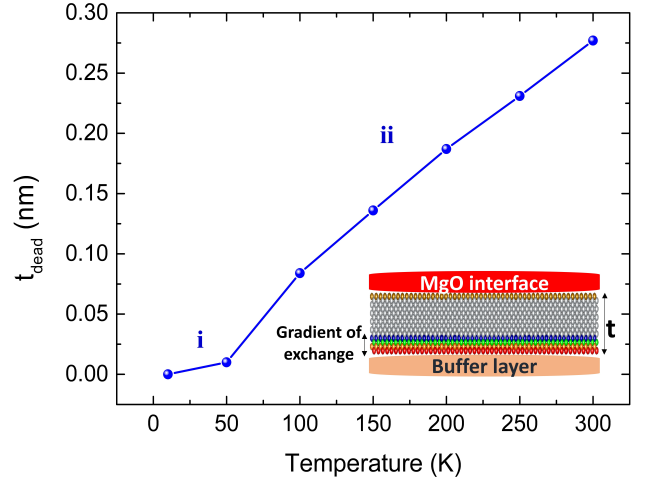


FIG. 5. (Color online) The variation of magnetic dead layer thickness t_{dead} plotted as a function of temperature shows two regimes: a negligible thickness regime denoted by i and another revealing an increase of t_{dead} with temperature (ii). The inset displays the structure used to model the dead layer comprising a region with a gradient of the exchange constant.

at sufficiently low temperatures [region (i) in Fig. 5] since the layers with exchange gradient still contribute a substantial saturation magnetization M_s . However, increasing the temperature results in the decrease of their M_s , which in turn increases the dead layer thickness [region (ii) in Fig. 5].

In order to check how the magnetic dead layer affects the correlation between temperature dependences of K and M_s , we calculated the scaling power as a function of thickness of the system presented in Fig 6. We compare two possibilities of realizing this correlation: fitting $K(T)$ either versus the total saturation magnetization of the sample $M_{total}(T)$ or versus the interfacial saturation magnetization $M_{Fe1}(T)$. In the latter case, $n = 3$ is ideally obtained independent of the sample's thickness. However, if $K(T)$ is scaled versus the saturation magnetization of the whole sample, n becomes dependent on the sample thickness and can be fitted exponentially as $n = n_{max}(1 - e^{-a(t-t_0)})$ where n_{max} is the saturation value of n as a function of increased thickness, a is the rate, and t_0 is the center. This can be understood since the $M_{total}(T)$ varies with thickness while $K(T)$ remains constant reflecting its interfacial character. Interestingly, for low thicknesses below 3 nm, the scaling power drops below 3. Thus, the low values of the experimental scaling powers reported earlier can be attributed to the non-consideration of the presence of a magnetic dead layer with scaling the anisotropy by the total magnetization of the sample rather than the magnetization of the interfacial layer only.

It is noteworthy to mention that modeling magnetic dead layers this way provides a qualitative insight of its influence on the temperature dependence of the magnetic properties of realistic samples. In other words, changing

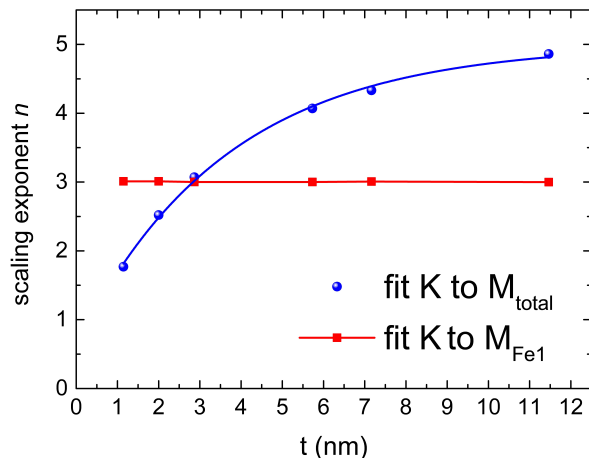


FIG. 6. (Color online) The effect of the magnetic dead layer on the temperature dependence of K is revealed by the variation of the scaling power n as a function of the magnetic layer thickness. The result of fitting K to the interfacial saturation magnetization (total saturation magnetization) M_{Fe1} (M_{total}) is shown by red squares (blue circles), respectively.

the gradient of exchange in our model would modify the values of the scaling exponents without changing the trend of its variation with the sample's thickness.

V. EFFECT OF INHOMOGENEITY IN PERPENDICULAR MAGNETIC ANISOTROPY

As we have already mentioned above, an analytical model [23, 26] and recent experiments [24, 28] pointed out to the presence of spatial fluctuations in the interfacial magnetic anisotropy. These fluctuations were attributed to local variations in the ferromagnetic layer thickness associated with film roughness or to the diffusion of buffer layer atoms through the ferromagnetic layer towards the MgO interface upon post-deposition annealing. Consequently, it is important to investigate the effect of inhomogeneous interfacial perpendicular magnetic anisotropy on its temperature dependence.

We thus employ the core shell model comprising two regions at the interface, one with a perpendicular (PMA) and the other possessing in-plane magnetic anisotropy as shown in the inset of Fig. 7. The resulting dependence as a function of the percentage of the interfacial PMA is shown in Fig. 7. One can see that the scaling power decreases as a function of interfacial PMA percentage regardless whether $K(T)$ is fitted to the total saturation magnetization of the sample $M_{total}(T)$ or to the interfacial saturation magnetization $M_{Fe1}(T)$ [Fig. 7]. This highlights that the effect of interfacial roughness plays also a crucial role in the temperature dependence of the magnetic properties of MgO-based interfaces and leads to deviations from the theoretical

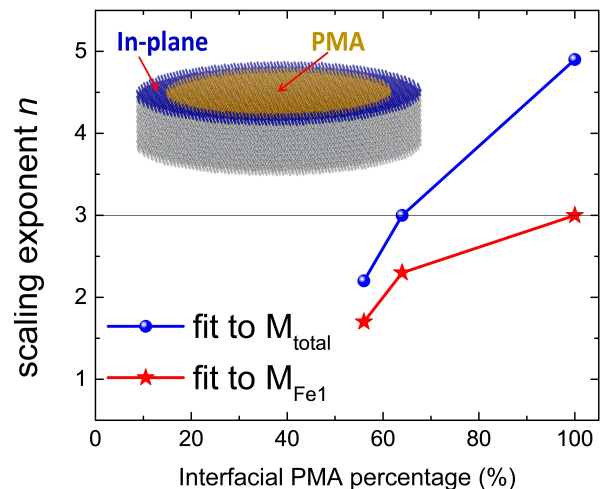


FIG. 7. (Color online) The variation of the scaling power n is plotted as a function of the percentage of interfacial PMA obtained by employing the core shell model shown in the inset. The result of fitting K to the interfacial saturation magnetization (total saturation magnetization) M_{Fe1} (M_{total}) is shown by red stars (blue circles), respectively.

Callen-Callen limit.

VI. CONCLUSION

The results presented in this work unveiled several important mechanisms for understanding of temperature dependence of magnetic anisotropy at MgO-based interfaces. Based on small second order anisotropy K_2 values obtained on the first-principles calculations, we ruled out an intrinsic origin of emergent higher-order anisotropy terms. Therefore, only the first order K_1 term was included in the atomistic spin Hamiltonian to describe the temperature dependence of the magnetic anisotropy. Fundamentally, it is important to distinguish between scaling interfacial $K(T)$ by the saturation magnetization of the whole magnetic layer or by the interfacial saturation magnetization only since they lead to different scaling powers. We found that the latter approach yields scaling power $n = 3$ per magnetic layer in agreement with Callen-Callen law. However, knowing that in experiments the total saturation magnetization scaling is used, the reported deviations from the Callen-Callen law can be thus understood including the variation of n on the sample's thickness. As a matter of fact, this dependence was observed in Ref. [32] at Co/AlOx₂ interface. In this respect, the deviations from theoretical scaling Callen-Callen power law can be attributed to two mechanisms: the presence of a magnetic dead layer and the spatial fluctuations of the interfacial PMA. Distinguishing between these two mechanisms experimentally might be possible by either of the following two ways: (i) Thickness-dependent

measurements can be performed knowing that the mechanisms yield different thickness-dependence of n ; (ii) Interface-sensitive techniques such as Mossbauer experiments with Fe doped interfacial layer can give access to the interfacial magnetization. Accordingly, if scaling $K(T)$ by the interfacial magnetization leads to $n = 3$ independently of the magnetic layer thickness, then a magnetic dead layer mechanism could be concluded. Otherwise, $n < 3$ scaling powers indicate an inhomogeneous interfacial PMA mechanism. We anticipate that the provided description of temperature dependence of magnetic properties at MgO-based interfaces will help for fundamental and technical understanding of thermal effects.

This work was partially funded by ERC Adv grant MAGICAL n°669204.

Appendix: Calculation Methods

Our first-principles calculations are based on the projector-augmented wave (PAW) method [33] as implemented in the VASP package [34–36] using the generalized gradient approximation [37] and including spin-orbit coupling within the second-order perturbation theory [38]. A kinetic energy cutoff of 550 eV has been used for the plane-wave basis set and a $31 \times 31 \times 1$ k -point mesh to sample the first Brillouin zone. The periodic structures comprises five magnetic monolayers (ML), Fe or FeCo, sandwiched between five ML of MgO. All the structures were fully relaxed in atomic positions and volume until the forces became smaller than 1 meV/Å. The layer-resolved magnetic anisotropy contributions are evaluated following [30].

The atomistic calculations are based on the classical atomistic spin model implemented in the VAMPIRE package [39, 40]. This allows to study the influence of thermal spin fluctuations on the intrinsic magnetic properties such as the magnetization and magnetic anisotropy. The spin Hamiltonian including the exchange interaction and the uniaxial magnetic anisotropy is written as:

$$H = - \sum_{i < j} J_{ij} \mathbf{S}_i \cdot \mathbf{S}_j - \sum_i k_u (\mathbf{S}_i \cdot \mathbf{e}_i)^2, \quad (\text{A.1})$$

where J_{ij} is the isotropic exchange constant between nearest-neighboring atomic sites of local spin moment directions \mathbf{S}_i and \mathbf{S}_j , k_u is the uniaxial anisotropy constant per atom, and \mathbf{e}_i is a unit vector along the

magnetic easy axis. Only the first order anisotropy constant is included in the Hamiltonian since our first-principles calculations demonstrated small second order K_2 values. To model the Fe/MgO interface, we construct a cylindrical-shaped system with a 15 nm diameter and varied thickness t from the body-centered cubic (bcc) Fe crystal of lattice parameter $a = 2.866$ Å. We divide the system into two regions: (i) bulk with negligible k_u and atomic spin moment of $2.2 \mu_B$, and (ii) interfacial region with an enhanced atomic spin moment of 2.76 (2.49) μ_B and $k_u = 1.099 \times 10^{-22}$ (4.593×10^{-23}) J/atom for the first Fe1 (second Fe2) monolayer, respectively. Those site-resolved magnetic anisotropy values, shown in Fig. 8, are based on our first-principles calculations revealing that the interfacial magnetic anisotropy in Fe/MgO is mainly contributed from the first and second Fe monolayers [30]. The exchange constant of Fe (bcc), $J_{ij} = 7.05 \times 10^{-21}$ J/link, obtained from the mean-field expression with the spin waves correction is used for both bulk and interfacial regions [39]. The constrained Monte-Carlo approach, as described in Ref. [41], is used to calculate the temperature-dependent saturation magnetization and anisotropy of the modeled system. We use 100,000 Monte-Carlo equilibration steps followed by 100,000 steps over which the thermodynamic averages are calculated to obtain the temperature-dependent system's properties.

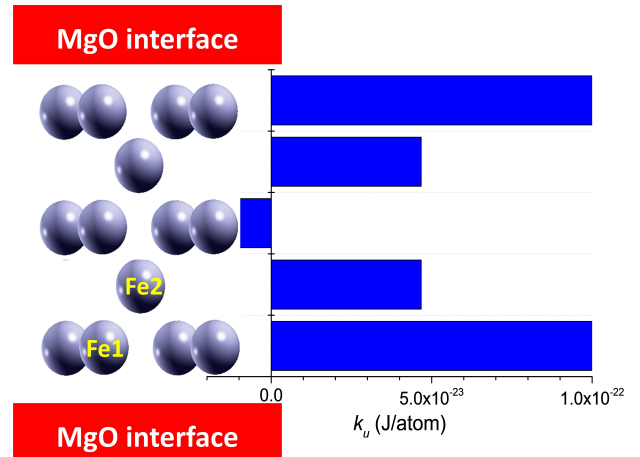


FIG. 8. (Color online) Layer-resolved anisotropy energies to first order k_u at MgO/Fe/MgO interface, obtained from first-principles calculations, showing that the both the first (Fe1) and second (Fe2) Fe monolayers contribute to the PMA. Those values are used to parameterize the temperature-dependent atomistic calculations.

-
- [1] J. C. Slonczewski, Current-driven excitation of magnetic multilayers, *Journal of Magnetism and Magnetic Materials* **159**, L1 (1996).
 - [2] L. Berger, Emission of spin waves by a magnetic

multilayer traversed by a current, *Physical Review B* **54**, 9353 (1996).

- [3] T. Kawahara, K. Ito, R. Takemura, and H. Ohno, Spin-transfer torque ram technology: Review and prospect,

- Microelectronics Reliability **52**, 613 (2012).
- [4] A. D. Kent and D. C. Worledge, A new spin on magnetic memories, *Nature Nanotechnology* **10**, 187 (2015).
 - [5] D. Apalkov, B. Dieny, and J. Slaughter, Magnetoresistive random access memory, *Proceedings of the IEEE, Institute of Electrical and Electronics Engineers* **104**, 1796 (2016).
 - [6] A. V. Khvalkovskiy, D. Apalkov, S. Watts, R. Chepulsii, R. S. Beach, A. Ong, X. Tang, A. Driskill-Smith, W. H. Butler, P. B. Visscher, D. Lottis, E. Chen, V. Nikitin, and M. Krounbi, Basic principles of stt-mram cell operation in memory arrays, *Journal of Physics D: Applied Physics* **46**, 074001 (2013).
 - [7] S. Ikeda, K. Miura, H. Yamamoto, K. Mizunuma, H. D. Gan, M. Endo, S. Kanai, J. Hayakawa, F. Matsukura, and H. Ohno, A perpendicular-anisotropy cofeb—mgo magnetic tunnel junction, *Nature Materials* **9**, 721–724 (2010).
 - [8] G. Jan, Y.-J. Wang, T. Moriyama, Y.-J. Lee, M. Lin, T. Zhong, R.-Y. Tong, T. Torng, and P.-K. Wang, High spin torque efficiency of magnetic tunnel junctions with mgo/cofeb/mgo free layer, *Applied Physics Express* **5**, 093008 (2012).
 - [9] B. Dieny and M. Chshiev, Perpendicular magnetic anisotropy at transition metal/oxide interfaces and applications, *Reviews of Modern Physics* **89**, 025008 (2017).
 - [10] B. Rodmacq, S. Auffret, B. Dieny, S. Monso, and P. Boyer, Crossovers from in-plane to perpendicular anisotropy in magnetic tunnel junctions as a function of the barrier degree of oxidation, *Journal of Applied Physics* **93**, 7513 (2003).
 - [11] A. Manchon, C. Ducruet, L. Lombard, S. Auffret, B. Rodmacq, B. Dieny, S. Pizzini, J. Vogel, V. Uhlir, M. Hochstrasser, and G. Panaccione, Analysis of oxygen induced anisotropy crossover in pt/co/mox trilayers, *Journal of Applied Physics* **104**, 043914 (2008).
 - [12] L. E. Nistor, B. Rodmacq, S. Auffret, and B. Dieny, Pt/co/oxide and oxide/co/pt electrodes for perpendicular magnetic tunnel junctions, *Applied Physics Letters* **94**, 012512 (2009).
 - [13] H. X. Yang, M. Chshiev, B. Dieny, J. H. Lee, A. Manchon, and K. H. Shin, First-principles investigation of the very large perpendicular magnetic anisotropy at fe—mgo and co—mgo interfaces, *Physical Review B* **84**, 054401 (2011).
 - [14] S. Bandiera, R. C. Sousa, M. M. de Castro, C. Ducruet, C. Portemont, S. Auffret, L. Vila, I. L. Prejbeanu, B. Rodmacq, and B. Dieny, Spin transfer torque switching assisted by thermally induced anisotropy reorientation in perpendicular magnetic tunnel junctions, *Applied Physics Letters* **99**, 202507 (2011).
 - [15] E. R. Callen and H. B. Callen, Static magnetoelastic coupling in cubic crystals, *Physical Review* **129**, 578 (1963).
 - [16] E. R. Callen and H. B. Callen, The present status of the temperature dependence of magnetocrystalline anisotropy, and the $1/(1+1/2)$ power law, *Journal of Physics and Chemistry of Solids* **27**, 1271 (1966).
 - [17] H. D. Gan, H. Sato, M. Yamanouchi, S. Ikeda, K. Miura, R. Koizumi, F. Matsukura, and H. Ohno, Origin of the collapse of tunnel magnetoresistance at high annealing temperature in cofeb/mgo perpendicular magnetic tunnel junctions, *Applied Physics Letters* **99**, 252507 (2011).
 - [18] J. G. Alzate, P. K. Amiri, G. Yu, P. Upadhyaya, J. A. Katine, J. Langer, B. Ocker, I. N. Krivorotov, and K. L. Wang, Temperature dependence of the voltage-controlled perpendicular anisotropy in nanoscale mgo—cofeb—ta magnetic tunnel junctions, *Applied Physics Letters* **104**, 112410 (2014).
 - [19] H. Sato, P. Chureemart, F. Matsukura, R. W. Chantrell, H. Ohno, and R. F. L. Evans, Temperature-dependent properties of cofeb/mgo thin films: Experiments versus simulations, *Physical Review B* **98**, 214428 (2018).
 - [20] O. N. Mryasov, U. Nowak, K. Y. Guslienko, and R. W. Chantrell, Temperature-dependent magnetic properties of fept: Effective spin hamiltonian model, *Europhysics Letters* **69**, 805 (2005).
 - [21] R. Skomski, O. N. Mryasov, J. Zhou, and D. J. Sellmyer, Finite-temperature anisotropy of magnetic alloys, *Journal of Applied Physics* **99**, 08E916 (2006).
 - [22] L. Cuchet, B. Rodmacq, S. Auffret, R. C. Sousa, and B. Dieny, Influence of magnetic electrodes thicknesses on the transport properties of magnetic tunnel junctions with perpendicular anisotropy, *Applied Physics Letters* **105**, 052408 (2014).
 - [23] B. Dieny and A. Vedyayev, Crossover from easy-plane to perpendicular anisotropy in magnetic thin films: Canted anisotropy due to partial coverage or interfacial roughness, *Europhysics Letters* **25**, 723 (1994).
 - [24] A. A. Timopheev, R. Sousa, M. Chshiev, H. Nguyen, and B. Dieny, Second order anisotropy contribution in perpendicular magnetic tunnel junctions, *Scientific Reports* **6**, 26877 (2016).
 - [25] B. M. S. Teixeira, A. A. Timopheev, N. F. F. Caçoiló, S. Auffret, R. C. Sousa, B. Dieny, E. Alves, and N. A. Sobolev, Ion irradiation-induced easy-cone anisotropy in double-mgo free layers for perpendicular magnetic tunnel junctions, *Applied Physics Letters* **112**, 202403 (2018).
 - [26] B. Heinrich, T. Monchesky, and R. Urban, Role of interfaces in higher order angular terms of magnetic anisotropies: ultrathin film structures, *Journal of Magnetism and Magnetic Materials* **236**, 339 (2001).
 - [27] J. Z. Sun, Consequences of an interface-concentrated perpendicular magnetic anisotropy in ultrathin cofeb films used in magnetic tunnel junctions, *Physical Review B* **91**, 174429 (2015).
 - [28] A. A. Timopheev, B. M. S. Teixeira, R. C. Sousa, S. Auffret, T. N. Nguyen, L. D. Buda-Prejbeanu, M. Chshiev, N. A. Sobolev, and B. Dieny, Inhomogeneous free layer in perpendicular magnetic tunnel junctions and its impact on the effective anisotropies and spin transfer torque switching efficiency, *Physical Review B* **96**, 014412 (2017).
 - [29] S. A. Khan, P. Blaha, H. Ebert, J. Minàr, and O. Sipr, Magnetocrystalline anisotropy of fept: A detailed view, *Physical Review B* **94**, 144436 (2016).
 - [30] A. Hallal, H. X. Yang, B. Dieny, and M. Chshiev, Anatomy of perpendicular magnetic anisotropy in fe/mgo magnetic tunnel junctions: First-principles insight, *Physical Review B* **88**, 184423 (2013).
 - [31] J. B. Mohammadi, K. Cole, T. Mewes, and C. K. A. Mewes, Inhomogeneous perpendicular magnetic anisotropy as a source of higher-order quasistatic and dynamic anisotropies, *Physical Review B* **97**, 014434 (2018).
 - [32] S. Bandiera, *Jonctions tunnel magnétiques à anisotropie*

- perpendiculaire et écriture assistée thermiquement*, Ph.D. thesis, Université de Grenoble (2011).
- [33] P. E. Blöchl, Projector augmented-wave method, *Physical Review B* **50**, 17953 (1994).
 - [34] G. Kresse and J. Hafner, Ab initio molecular dynamics for liquid metals, *Physical Review B* **47**, 558 (1993).
 - [35] G. Kresse and J. Furthmüller, Efficient iterative schemes for ab initio total-energy calculations using a plane-wave basis set, *Physical Review B* **54**, 11169 (1996).
 - [36] G. Kresse and J. Furthmüller, Efficiency of ab-initio total energy calculations for metals and semiconductors using a plane-wave basis set, *Computational Materials Science* **6**, 15 (1996).
 - [37] J. P. Perdew, K. Burke, and M. Ernzerhof, Generalized gradient approximation made simple, *Physical Review Letters* **77**, 3865 (1996).
 - [38] G. van der Laan, Microscopic origin of magnetocrystalline anisotropy in transition metal thin films, *Journal of Physics: Condensed Matter* **10**, 3239 (1998).
 - [39] R. F. L. Evans, W. J. Fan, P. Chureemart, T. A. Ostler, M. O. A. Ellis, and R. W. Chantrell, Atomistic spin model simulations of magnetic nanomaterials, *Journal of Physics: Condensed Matter* **26**, 103202.
 - [40] Vampire software package, version 5, <http://vampire.york.ac.uk/>.
 - [41] P. Asselin, R. F. L. Evans, J. Barker, R. W. Chantrell, R. Yanes, O. Chubykalo-Fesenko, D. Hinzke, and U. Nowak, Constrained monte carlo method and calculation of the temperature dependence of magnetic anisotropy, *Physical Review B* **82**, 054415 (2010).